AGU PUBLICATIONS

Geophysical Research Letters

RESEARCH LETTER
10.1002/2016GL071220

Key Points:
- Prethaw carbon flux pulses during thaw offset 46% of CO_2 summer uptake and added 6% to CH_4 summer fluxes
- Laboratory experiment linked pulse emissions to a delayed microbial production mechanism
- The spring pulse may be a large underrepresented source of carbon in Arctic regions

Correspondence to:
N. Raz-Yaseef,
nryaseef@lbl.gov

Citation:
Raz-Yaseef, N., M. S. Torn, Y. Wu, D. P. Billesbach, A. K. Liljedahl, T. J. Kneafsey, V. E. Romanovsky, D. R. Cook, and S. D. Wullschleger (2017), Large CO_2 and CH_4 emissions from polygonal tundra during spring thaw in northern Alaska, *Geophys. Res. Lett.*, *44*, 504–513, doi:10.1002/2016GL071220.

Received 16 SEP 2016
Accepted 23 NOV 2016
Accepted article online 5 DEC 2016
Published online 10 JAN 2017

Large CO_2 and CH_4 emissions from polygonal tundra during spring thaw in northern Alaska

Naama Raz-Yaseef[1], Margaret S. Torn[1,2], Yuxin Wu[1], Dave P. Billesbach[3], Anna K. Liljedahl[4], Timothy J. Kneafsey[1], Vladimir E. Romanovsky[5], David R. Cook[6], and Stan D. Wullschleger[7]

[1]Climate and Ecosystem Sciences Division, Lawrence Berkeley National Laboratory, Berkeley, California, USA, [2]Energy and Resources Group, University of California, Berkeley, California, USA, [3]Biological Systems Engineering Department, University of Nebraska–Lincoln, Lincoln, Nebraska, USA, [4]Water and Environmental Research Center, University of Alaska Fairbanks, Fairbanks, Alaska, USA, [5]Geophysical Institute, University of Alaska Fairbanks, Fairbanks, Alaska, USA, [6]Environmental Science Division, Argonne National Laboratory, Lemont, Illinois, USA, [7]Environmental Sciences Division, Oak Ridge National Laboratory, Oak Ridge, Tennessee, USA

Abstract The few prethaw observations of tundra carbon fluxes suggest that there may be large spring releases, but little is known about the scale and underlying mechanisms of this phenomenon. To address these questions, we combined ecosystem eddy flux measurements from two towers near Barrow, Alaska, with mechanistic soil-core thawing experiment. During a 2 week period prior to snowmelt in 2014, large fluxes were measured, reducing net summer uptake of CO_2 by 46% and adding 6% to cumulative CH_4 emissions. Emission pulses were linked to unique rain-on-snow events enhancing soil cracking. Controlled laboratory experiment revealed that as surface ice thaws, an immediate, large pulse of trapped gases is emitted. These results suggest that the Arctic CO_2 and CH_4 spring pulse is a delayed release of biogenic gas production from the previous fall and that the pulse can be large enough to offset a significant fraction of the moderate Arctic tundra carbon sink.

1. Introduction

Pan-Arctic climate has warmed significantly over the last several decades, and end-of-20th-century Arctic warming exceeded global rates [*Spielhagen et al.*, 2011]. It is estimated that more than ~1300 Pg (±1100 Pg) of organic carbon are stored in the frozen tundra [*Hugelius et al.*, 2014], holding the potential for substantial emissions of CO_2 and CH_4 upon thawing [*Schadel et al.*, 2016], and thus for large positive feedback with climate change [*Schuur et al.*, 2015]. The Arctic is a significant methane source due to the abundance of saturated and inundated areas [*Walter et al.*, 2007], and a moderate CO_2 sink [*Ueyama et al.*, 2013], but current flux rates are uncertain, as are the controls [*McGuire et al.*, 2012]. One of the challenges in determining the carbon balance of Arctic regions is the difficulty in quantifying winter and shoulder season fluxes, from freeze-in to thaw. While plant CO_2 uptake occurs only in the summer, microbial activity can continue for weeks or even months after light and temperature limit photosynthesis [*Jansson and Taş*, 2014]. Indeed, measurements during the nonsummer months have recently shown that emissions are significant both for CO_2 [*Oechel et al.*, 2014] and for CH_4 [*Zona et al.*, 2015]. Because of the low biomass and short active season of tundra vegetation, efflux during the winter and shoulder seasons may have significant consequences for annual carbon budgets of the Arctic [*Belshe et al.*, 2013]. Most observational studies of shoulder-season emission pulses have focused on the fall freezeup season for CO_2 pulses [*Fahnestock*, 1999; *Bubier et al.*, 2002], CH_4 pulses [*Hargreaves et al.*, 2001; *Wille et al.*, 2008], or a combination of both CO_2 and CH_4 fall pulses [*Tagesson et al.*, 2012; *Mastepanov et al.*, 2013].

Only a few studies have observed spring-thaw pulses to date, most focusing on episodic CH_4 pulses, with even less information available on CO_2 pulses. *Moore and Knowles* [1990] and *Windsor et al.* [1992] have measured CH_4 year-round fluxes in Quebec by using soil chambers and found that episodic spring fluxes increased the annual budget by 7–22%. *Song et al.* [2012] measured a large spring CH_4 pulse with soil chambers in China: a 2 day thaw event released CH_4 fluxes that were equal to 80% of the active season fluxes. Episodic spring CH_4 fluxes measured with soil chambers were also reported by *Nykänen et al.* [2003] in Finland and *Tokida et al.* [2007] in Japan. *Friborg et al.* [1997] and *Hargreaves et al.* [2001] measured CO_2 and CH_4 fluxes with flux towers in Sweden and Finland, respectively, and reported CH_4 spring pulses that

were up to 25% of midsummer fluxes and up to 11% of the annual budget, respectively. *Friborg et al.* [1997] reported CO_2 spring fluxes of up to 500 mg m^{-2} h^{-1}, but the contribution to the annual budget could not be determined. Others reported on carbon spring fluxes that were small and insignificant (*Wille et al.* [2008]: flux tower in Siberia, CH_4 spring pulses accounted for 3% of the active season flux; *Tagesson et al.* [2012]: flux tower in Greenland, small CH_4 and CO_2 flux pulses were detected in spring; and *Mastepanov et al.* [2013]: soil chambers measurements in Greenland, small CH_4 and CO_2 flux pulses were detected in spring).

To provide a more in-depth understanding of greenhouse gas emissions on the North Slope of Alaska, we employed a multiscale approach in the field and the laboratory. We combined ecosystem-scale measurements from two eddy flux towers, local measurements of soil temperature and soil gas concentrations, and a controlled soil-core thawing laboratory experiment. The study allowed us to link the source, mechanism, and magnitude of spring pulses of CO_2 and CH_4 from thawing permafrost tundra on the North Slope of Alaska.

2. Methods

2.1. Field Site

Our field site is located near the village of Barrow, Alaska, on the shores of the Beaufort and Chukchi Seas, approximately 400 km north of the Brooks Range. The main research site is operated by the U.S. Department of Energy (DOE) Next Generation Ecosystem Experiment (NGEE) and is located on the Barrow Environmental Observatory (BEO, 71.29°N, 156.61°W). Here, an eddy tower was installed, soil temperature was measured, and the soil cores were taken. The secondary research site is located 4 km to the north and is operated by the U.S. DOE Atmospheric Radiation Measurement Program (ARM, 71.32°N, 156.60°W), where an eddy tower was also erected.

The Arctic coastal plain is a relatively flat polygonal tundra. Polygons are geometrical ground features surrounded by troughs and formed by growing or decaying ice wedges. The elevation differences between edges and troughs of polygons are roughly 1 m [*Hubbard et al.*, 2012]. The region is underlain by thick continuous permafrost, and the summer active layer is limited to a maximum depth of approximately 50 cm [*Gangodagamage et al.*, 2014]. Mean annual air temperature is −12°C, and mean annual precipitation is 114 mm, with the majority falling as rain during the short summer (1901–2007). Soils in the BEO are highly porous and have high organic content and high water holding capacity [*Brown et al.*, 1980]. The soil can be divided into an organic-rich surface layer 5 to 20 cm thick (depending on location [*Hubbard et al.*, 2012]) underlain by a mineral soil horizon of silty clay to silt loam-textured-mineral material, together comprising the "active layer." The "permafrost," a perennially frozen layer, extends from an average depth of 50 cm down to ~600 m [*Hubbard et al.*, 2012]. The vegetation at Barrow is a mixture of vascular plants such as sedge (*Carex aquatilis*) and nonvascular constituents such as moss (mainly Sphagnum sp.) and lichens (such as *Dactylina arctica*) [*Sturtevant and Oechel*, 2013; *Wullschleger et al.*, 2014].

2.2. Flux Measurements

To measure CO_2 and CH_4 fluxes at ecosystem scale (hundreds of meters), eddy covariance towers were installed at the ARM site in September 2011 and at the BEO site in September 2012. Because the icy winter conditions compromise the eddy covariance instruments, the BEO eddy covariance system was nonoperational and the ARM system was minimally operational from mid-November to early May. Only in 2014 were both systems functioning during the spring thaw period.

The main instruments in both systems are Gill-Solent sonic anemometers (WindMaster Pro at the ARM site and R3-50 at the BEO site), LI-COR CO_2/H_2O open-path infrared gas analyzers (IRGA; LI-7500 at the ARM site, and LI-7500A at the BEO site), and LI-COR LI-7700 open-path CH_4 tunable diode laser absorption spectroscopy (TDLAS). Instruments were located about 4 m above the ground. Both of these instrument systems were connected to the network for daily delivery of raw data to our laboratory in Lincoln, Nebraska. Because of network security issues, the ARM instruments were not always accessible for routine maintenance and cleaning, resulting in significant data loss.

During the nonoperational months, the trace gas instruments were returned to the laboratory for cleaning, maintenance, and calibrations. Trace gas analyzers from both systems showed little annual change between

years. Small changes in offsets, attributed to accumulation of contaminants on optical windows and mirrors (which were cleaned periodically during the deployments), were removed in data postprocessing.

Raw data were postprocessed to yield fully corrected, half-hourly, high-quality fluxes of CH_4, CO_2, latent and sensible heat, and momentum (friction velocity) [*Lee et al*, 2004]; flux uncertainties [*Billesbach*, 2011]; and QA/QC indicators. First, raw data were scanned for spikes and outliers, and data points that were more than six standard deviations from the mean of a moving window (approximately 20 min wide) were replaced by the mean value. Then, data were scanned for gaps or missing points. Half-hour periods with more than 200 (out of 18,000) missing or replaced data points were rejected. Next, wind speed data were coordinate-rotated to zero the mean vertical wind speed and the mean cross wind speed, and the block averages (30 min periods) of all data streams were removed to generate fluctuations. IRGA and TDLAS data streams were time-shifted to resynchronize them with the sonic anemometer data by maximizing the covariance between each instrument and the vertical wind speed fluctuations as a function of delay time. Finally, statistics (e.g., means, variances, covariances, skewness, and kurtosis) and fluxes were calculated. To produce final fluxes, ancillary factors were calculated and applied (such as the effect of water-vapor transfer on sonic temperature and sensible heat flux, Webb-Pearman-Leuning terms, quantum line-broadening of CH_4 absorption lines, WindMaster Pro "w-boost," and corrections for imperfect frequency response and finite separation of the sensors). Uncertainty estimates (variance of the covariance) were generated for each covariance. These were then propagated through the appropriate relationships to produce uncertainty estimates for the final fluxes [*Billesbach*, 2011]. The uncertainties in the individual, validated fluxes define a confidence limit to the associated flux value and were approximately 10%. The programs used for data processing have been fully verified against the AmeriFlux Gold Files through several AmeriFlux intercomparison studies (at other sites) over 15 years of use.

To estimate total emissions during the pulse events, Gaussian fits (on non-gap-filled data) were performed over the time periods where pulses were observed. To estimate flux budgets over the season, we filled gaps in the CO_2 and CH_4 record by using a method based on marginal distribution sampling (MDS) [*Reichstein et al*., 2005], in which a missing data point is assigned a value based on measured data points with similar micrometeorological conditions. This method was not applied to the pulse periods because it was not appropriate to assume continuous behavior, and application of the MDS method would underestimate pulse values due to their unique and sporadic nature.

2.3. Soil Temperature

To measure soil temperature, replicates of subsurface temperature measurements were made along transects between polygon centers and troughs. Transects were installed at five different locations at the BEO, each measuring at five distinct points (polygon center, off-center, first rim, trough, and second rim). A vertical array of thermistors installed at every measurement point measured 16 depth points from the surface to 1.5 m depth. Temperature was measured every 5 min year-round. Hourly average values were stored on a Campbell Scientific CR1000 data logger. Prior to installation, the thermistors were calibrated in an ice bath to an accuracy of approximately ± 0.02°C at 0°C. Soil temperatures used in this study are an average of all measurements for three defined soil layer intervals (shallow: 2–15 cm, medium: 15–50 cm, and permafrost: 50–150 cm).

2.4. Soil Cores

To investigate soil structure and conduct controlled laboratory experiments, frozen 10 cm diameter soil cores were extracted from a low-centered polygon area at the BEO. Cores were taken in April 2013, when the complete soil profile was frozen, to assure that frozen conditions were maintained and to protect the soil structure. The cores were extracted from the surface to a depth of 70 cm and transported to the laboratory while frozen.

2.4.1. Thaw Experiment

To measure gas emissions under controlled conditions, a core was thawed in the laboratory from the surface down under precise temperature control. This was achieved by regulating the temperature of a heating element approximately 1 cm above the core surface. Thermocouples (type T) were installed along the column length to monitor temperature changes and track the thawing front over time. The headspace of the soil column was constantly purged with zero air (CO_2 free) at constant rate. Gases emitted from the soil and purged out with zero air were sampled every 2–6 days with nonpermeable Cali-5-bond gas sampling bags

Table 1. Carbon Fluxes (Total Values and Estimated Error) Measured During the Thaw Event (Spring Pulse) and the Active Plant Summer (Snow-Free Season)[a]

Period	Date	CO_2 (mmol m^{-2})	CH_4 (mmol m^{-2})
Pulse #1	18/5/2014	23.9 ± 8.4	0.5 ± 0.1
Pulse #2	21–22/5/2014	42.5 ± 16.3	1.0 ± 0.2
Pulse #3	29/5/2014 to 2/6/2014	510.3 ± 85.5	7.0 ± 0.8
Total spring pulse	18/5/2014 to 2/6/2014	576.7 ± 110	8.5 ± 1.0
Snow-free season	9/6/2014 to 27/9/2014	-1245 ± -485	136 ± 18

[a]Negative CO_2 fluxes denote net ecosystem carbon uptake. Fluxes during the 2 week spring pulse offset 46% of the summer CO_2 uptake and added 6% to the summer CH_4 efflux.

(Calibrated Instruments, Inc.). The gas collector bag was only installed during the sampling event, which typically lasted 6–8 h per sample. The collected gas was analyzed by gas chromatography by using a Shimadzu Gas Chromatography (model GC-2014). The experiment was conducted in a temperature-controlled incubator kept below 0°C at all times.

2.4.2. X-ray Computed Tomography Scans

Computed tomography (CT) scans are often used to evaluated the structures of the active layer and the permafrost [*Orsi et al.*, 1996; *Taina et al.*, 2008]. Similarly, we used available CT scans conducted on nearly 100 cores collected from various locations and depths at the BEO. All cores were collected when the ground was frozen, and were shipped and scanned frozen. Cores were scanned by using a modified third-generation medical X-ray computed tomography (General Electric Lightspeed 16). Bulk density was estimated by using the CT data and based on a calibration curve made from scanning known-density materials.

2.5. Gas Tubes

To measure CO_2 and CH_4 concentrations in the soil, soil gas was periodically collected from stainless steel probes (0.635 cm diameter) inserted in the soil to depths of 10 cm and 20 cm at the BEO in June 2013. The probes were sealed with airtight caps. During sampling, soil gas was manually collected into syringes by a needle inserted through a septa in the cap. Gas samples were injected directly into evacuated vials. CO_2 and CH_4 concentrations were quantified by using a GC- 2014 Shimadzu gas chromatograph.

2.6. Precipitation and Snow Cover

Long-term records (1949–2014) of daily precipitation and mean air temperature were retrieved from the National Climatic Data Center Web archive for the Barrow Airport (STN 700260 and WBAN 27502), located approximately 7 km from the eddy flux towers. Adjustments for undercatch, which is caused by wind, wetting, and trace, were made to daily rain and snowfall according to the methods by *Yang et al.* [1998]. Rain on snow (ROS) was defined as adjusted daily precipitation during the months of October through May when average daily air temperature exceeded −1°C.

Snow depth measurements were made daily throughout the snowmelt period along a 1 km east-west transect (start 71°17.02′N, −156°35.34′, end 71°17.12′N, −156°34.70′E). Snow depths were measured every ~1 m along the transect by using a MagnaProbe (SnowHydro) that allowed for ~1000 depth measurements per day. The snow-covered area (%) was calculated from the number of snow depth measurements with nonzero values divided by the total number of snow depth measurements.

3. Results

During early spring of 2014, the NGEE eddy tower recorded periods of large fluxes of CO_2 and CH_4, with up to 6.5 μmol CO_2 m^{-2} s^{-1} and 53 nmol CH_4 m^{-2} s^{-1} (Table 1 and Figures 1a and 1b). Between 18 May and 2 June, three distinct pulses of CO_2, CH_4, and sensible heat (but not latent heat) were observed, with the longest and largest lasting 5 days. On the same days, pulses of similar size and duration were observed at the ARM eddy tower site 4 km away (Figures 1c and 1d).

At the time of the observed flux pulses, the average air temperature and soil temperature were still below freezing, and the surface was mostly covered with snow (Figure 2). Prior to the pulse event, a series of warming and cooling cycles took place (Figure 2). Between 1 and 3 May, soil temperatures at 2 cm rose from −10°C to −4°C. Soon after, soil temperatures dropped to −7°C (9 May). Between 11 and 18 May soil temperatures at

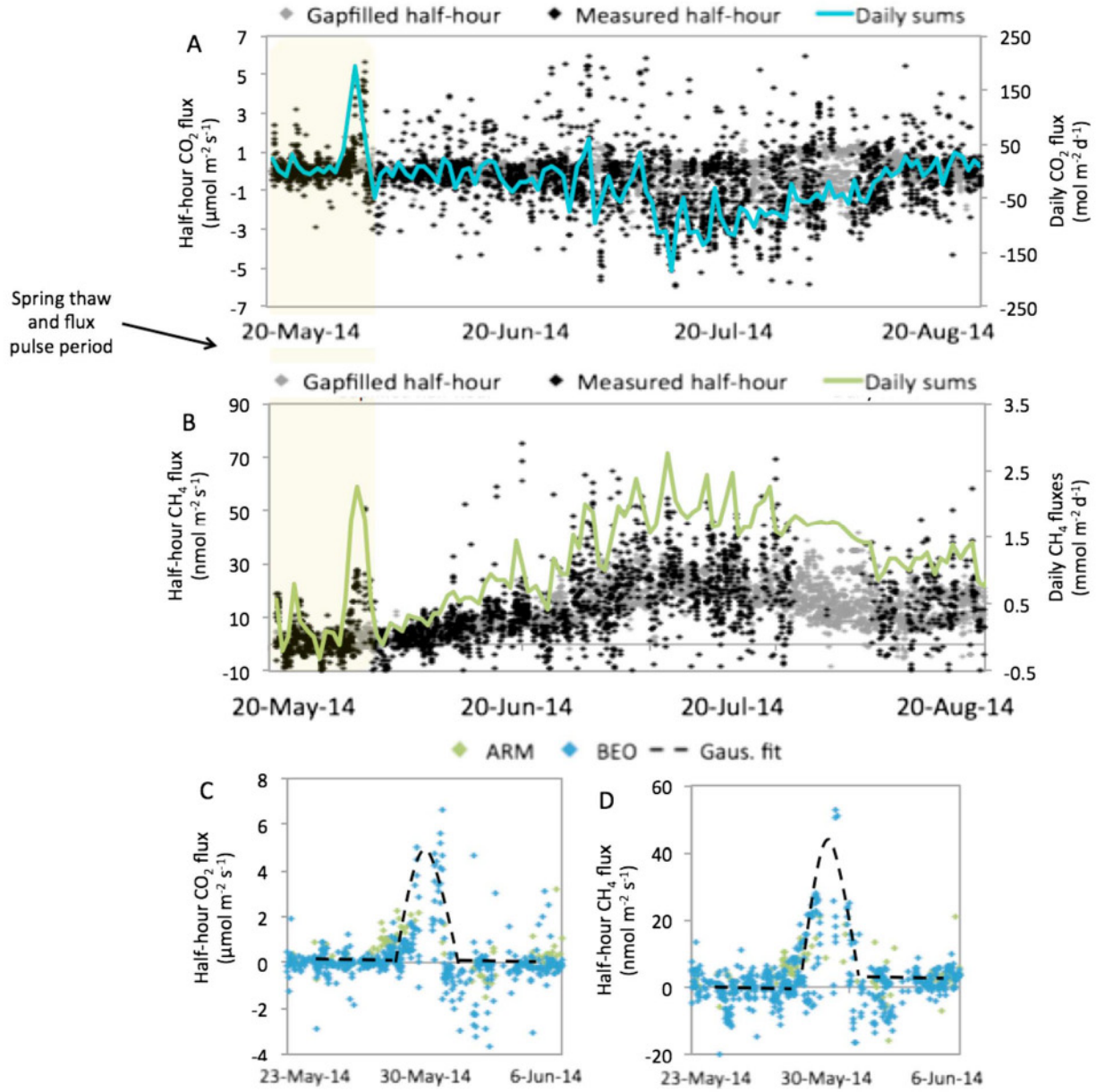

Figure 1. Eddy covariance fluxes measured near Barrow, AK. (a) CO_2 fluxes (measured half hourly: black diamonds, gap-filled half hourly: gray diamonds, daily totals: blue line). (b) CH_4 fluxes (measured half hourly: black diamonds, gap-filled half hourly: gray diamonds, daily totals: green line). (c) Half-hourly fluxes of CO_2 during the main spring pulse event at the two eddy covariance sites (ARM: green diamonds, BEO: blue diamonds, Gaussian fit: dashed line). (d) Half-hourly fluxes of CH_4 during the main spring pulse event at the two eddy covariance sites (ARM: green diamonds, BEO: blue diamonds, Gaussian fit: dashed line).

2 cm warmed from −6°C to near 0°C. These rapid warming cycles included rain on snow (ROS) events: 1.7 mm rain on 1 May, and an extreme rain event of 17.3 mm between 11 and 15 May. Photos taken with Web cameras showed that during this period sporadic snowmelt took place, exposing patches of soil that were then re-covered by snow (Figure 2).

Soon after the pulse events, fluxes returned to near zero until the ground became mostly snow-free (50% snow cover on 9 June). After that, the ecosystem shifted to the typical seasonal pattern of a gradual increase in CH_4 release and CO_2 uptake. Carbon uptake (negative fluxes of net ecosystem exchange (NEE)) peaked in late July, with fluxes up to $-6.0\,\mu mol\,m^{-2}\,s^{-1}$. Methane release peaked later, in early August, with fluxes up to $70\,nmol\,m^{-2}\,s^{-1}$. NEE gradually decreased until the ecosystem became a source for

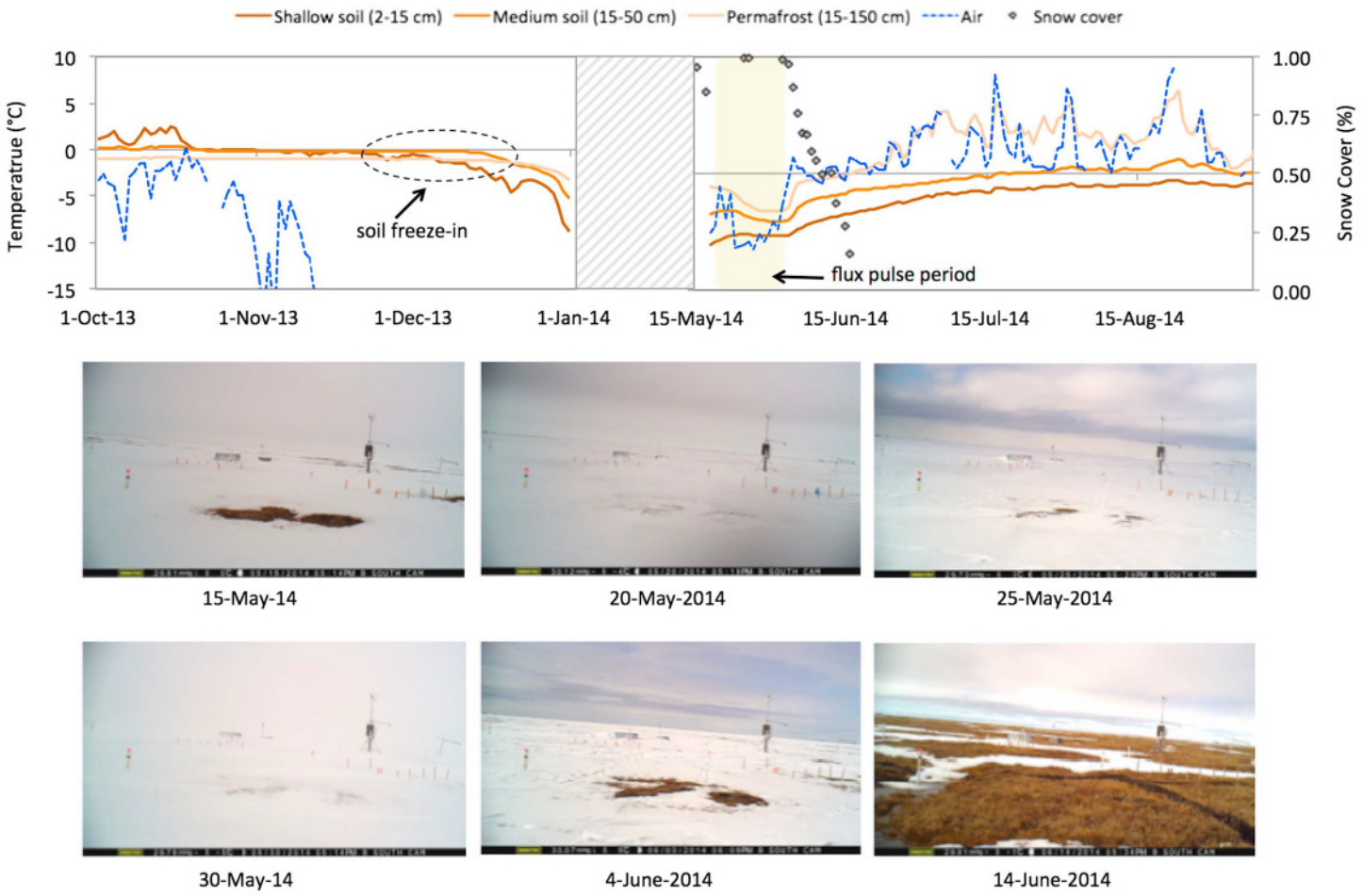

Figure 2. Air temperature and soil temperature averaged for shallow depth (2–15 cm), the midlayer (15–50 cm), and permafrost (50–150 cm). (left) The fall and freeze-in seasons are shown; winter is discontinued, and (right) the spring-thaw and summer seasons are also presented. Measurements of snow cover (%) and photos taken at the BEO prior and during snowmelt are also shown.

CO_2 (positive fluxes of NEE) at the end of August, approximately 2 weeks before freeze-in. Near-zero fluxes of CH_4 were observed during freeze-in in mid-September.

Cumulative fluxes during the 2014 snow-free period (June to September) show that the tundra ecosystem was a moderate sink for CO_2, with a net uptake of -1245 mmol CO_2 m^{-2}, and a source of atmospheric CH_4 of 136 mmol CH_4 m^{-2}. We estimate that the Barrow spring thaw pulses released 8.5 mmol CH_4 m^{-2} and 577 mmol CO_2 m^{-2}, based on a Gaussian fit to the pulse data (Table 1), amounting to more than 6% of total CH_4 summer fluxes and offsetting 46% of the total CO_2 summer sink (June to September). Although methane emission rates were much higher during the pulse than in the rest of the season, their contribution to the season total was small because the pulse season is short compared to the longer summer period, in which the site is a fairly large methane source.

To investigate the thaw-pulse mechanism, we performed a controlled laboratory experiment in which an intact frozen soil core collected in the BEO was gradually thawed from the top down (Figure 3a). As soon as the surface ice layer of the core had melted, high CO_2 and CH_4 emissions were observed (Figures 3b and 3c). Emissions continued as thawing progressed into the organic-rich layer of the soil column and dropped dramatically to near zero when thaw depth passed the upper 5 cm of the organic-rich layer and progressed into the mineral soil below. These results show that one source of the flux pulse could be a release of gas that was stored over winter in the organic horizon and released during thaw. The CT scans of many cores collected in the BEO revealed that the top 10 cm of the frozen soils were riddled with gas-rich channels and pockets (Figure 3d). These structures have much lower density than that of ice or the mineral

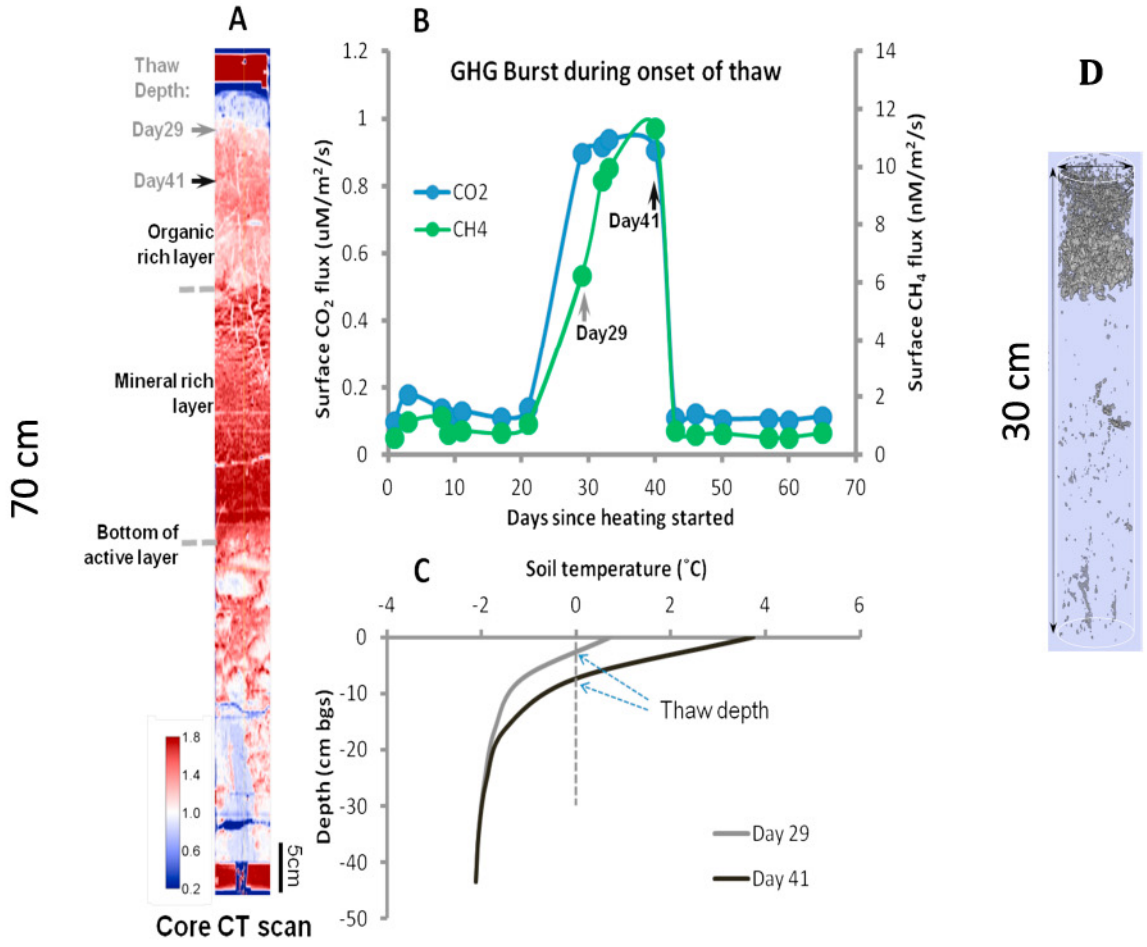

Figure 3. Results from a laboratory soil core warming experiment. (a) CT (computed tomography) scan of the Barrow core used for the experiment showing the soil density structure. Thaw depth during the carbon pulse (days 29 to 41) is marked. (b) CO_2 and CH_4 fluxes during the pulse that lasted ~12 days. (c) Temperature profile of the soil column at the beginning (day 29) and end (day 41) of the carbon pulse indicating thaw depths. (d) A CT scan of the upper 30 cm of a core, showing regions having soil densities lower than that of ice, i.e., trapped gas bubbles (darker color).

matrix (i.e., they were not ice-filled) and could serve as accumulation zones and enhanced pathways for gas flow in frozen and thawing soils.

The seasonal pattern in soil temperature profiles at the BEO is consistent with the accumulation of CO_2 and CH_4 in the soil in fall and winter. Snow and surface ice cover the ground typically from mid-October. Beneath the surface ice layer and above the permafrost, at a depth interval of roughly 10 to 40 cm, temperatures remain above or at the freezing point for another month or more after the surface layer has frozen (Figure 2). This middle layer gradually freezes from the surface down and the bottom up, until the complete soil profile is frozen in mid-December.

During the winter months of 2013–2014, a basal ice layer up to 5 cm thick was observed at the BEO, covering the soil. Soil-gas CO_2 and CH_4 concentrations beneath the newly frozen surface in fall were much higher than any seen during the growing season (Table 2). The average CO_2 concentrations in November 2013 were 7 times higher, and the average CH_4 concentrations were 1770 times higher than the average for the growing season (July–September 2014; Table 2).

4. Discussion

In this study, spring pulses of carbon gas efflux were observed in 2014 at the scales of a single soil column and of a flux-tower footprint. We report the first observations of replicated spring carbon pulses at the ecosystem scale. While spring-thaw pulses could result from rapid, short-term spin-up of microbial production

Table 2. Greenhouse Gas Concentrations Measured in Gas Samples Collected From Soil Pores at Depth of 10 and 20 cm[a]

		CO_2 (ppm)		CH_4 (ppm)	
Month	*n*	Mean	SE	Mean	SE
July	2	5,716	609	82	48
August	13	7,634	2,068	50	24
September	5	3,021	898	2	1
October	4	1,724	662	8	2
November	16	31,713	15,972	62,447	33,764

[a]The number of samples (*n*) and standard error (SE) are also shown. Highest concentrations were measured in November, after freeze-in. Mean concentrations for November were 7 times higher for CO_2 and 1770 times higher for CH_4 than those measured during July to October.

stimulated by the thaw, the pulse in the controlled laboratory experiment and a wide range of field observations all point to CO_2 and CH_4 production in the previous fall being the source of the pulses. Thus, it is more likely that the pulse is caused by the release of gases trapped in the frozen soils over winter [*Hargreaves et al.*, 2001; *Song et al.*, 2012].

In permafrost regions, microbial production can persist in fall and early winter in a temporarily unfrozen midlayer [*Oechel et al.*, 1997; *Jansson and Taş*, 2014; *Zona et al.*, 2015]. After the complete soil profile freezes, the resulting CO_2 and CH_4 can get trapped over winter between the underlying permafrost and the capping surface ice. Seasonal patterns in soil temperature (Figure 2) and measurements of high soil gas concentration in the fall (Table 2) confirm that fall soil carbon production and winter soil carbon storage take place at our field site.

At the BEO, widespread snowmelt is a rapid event, and in 2014 snow cover dropped from 99% to 16% between 2 and 16 June. The emission pulses were measured prior to snowmelt, from 18 May to 2 June, when air and soil temperatures were still well below zero. We conclude that the emission pulses were caused by a series of short, rapid cycles of warming and cooling prior to widespread snowmelt and thaw. Reoccurring and rapid temperature changes intensify soil cracking and may have triggered the emission pulse. The rain on snow events at the beginning of each of these warming cycles enhanced the amplitude and speed of the warming. In soil patches where snowmelt took place, the soil was temporarily exposed, the ice cover melted, and trapped gases were likely to be released. Although this snowmelt was neither terminal nor widespread, it occurred throughout the site, and measurable runoff was detected on 17 May. Evidence of ground cracking is found in CT scans of soil cores from the BEO, similar to *Pirk et al.* [2015], and could provide pathways for gas transport. In this sense, the spring pulse gas transport is similar to that of diffusion of CH_4 through plant aerenchyma [*Torn and Chapin*, 1993; *von Fischer et al.*, 2010]. In both cases, the rapid bypass of oxic, microbially active layers reduces methanotrophy.

Since the observed depth-pattern of freezeup is ubiquitous in permafrost soils [*Romanovsky and Osterkamp*, 2000], the entrapment of microbially produced CO_2 and CH_4 in soil over winter may be a pan-Arctic phenomenon, in which gas is trapped [*Fahnestock*, 1999] during the freezing of the active layer downward from the surface and upward from the permafrost. Indeed, the simultaneous signals we observed at both the BEO and the ARM eddy-covariance towers indicate that spring carbon pulses occur at scales that can be observed by ecosystem-scale measurements (although the releases themselves may occur at pore-to-core scale).

The scarcity of reported spring pulse events, however, raises two issues. First, it draws attention to the potential rarity of this phenomenon. At our field site, spring pulses were not detected in 2013 or in 2016; due to technical failure, the prethaw and thaw seasons were not measured in 2015. The lack of reports of spring pulses occurring in multiple years at the same site suggests that a set of conditions is required. Our research points to a few conditions that might favor spring pulse production: moist soils or wet surface at the end of summer to form an ice cap, unfrozen midsoil layer for at least several weeks to allow for microbial production in fall, and a series of rapid warming and cooling cycles in early spring, possibly associated with rain over snow events, to enhance soil cracking and allow for rapid gas release. Second, there are a few sites and fewer years of prethaw flux data from anywhere in the Arctic. Thus, the frequency and extent of these large pulses, and their impact on Arctic carbon budgets and process studies, are highly uncertain.

The large time lags between microbial production and observed emissions mean that an annual emissions budget in one calendar year depends on trace gas production in the previous year. Moreover, the large

temporal disconnects between the ecosystem drivers controlling production versus emission processes greatly complicate the use of flux and microclimate data to test land models, which typically assume synchronous control. In terms of budgets, this implies that CO_2 flux measurements starting after the spring thaw could overestimate the summertime Arctic carbon sink by as much as 50%. If small fluxes of CO_2 occur in the winter, as they do for CH_4 [*Zona et al.*, 2015], then the overall CO_2 sink may be lower still. Similarly, it is important to carefully measure and consider possible fall freezeup pulses [*Fahnestock*, 1999; *Hargreaves et al.*, 2001; *Bubier et al.*, 2002; *Mastepanov et al.*, 2008; *Wille et al.*, 2008; *Tagesson et al.*, 2012] when calculating tundra carbon budget. To date, episodic releases in fall have not been measured at our site.

The spring pulse is a significant, underrepresented source of CO_2 in Arctic carbon budgets. The dynamics of this offset in the context of climate change are not yet known, but it appears that while warming and CO_2 fertilization may lead to a longer and more productive growing season, a longer and warmer fall and early winter may increase the duration of the active layer freezing period, which will increase microbial activity [*Natali et al.*, 2015] and soil greenhouse gas storage. Further, there has been a gradual and steady increase in May rain on snow (ROS) events in Barrow in recent decades. There were barely any ROS events between 1949 until 1980. The average ROS for May was 1 mm in the 1980s, 3 mm in the 1990s, 2 mm in the 2000s, and 9 mm between 2011 and 2014. The total amount of ROS for the springmelt in 2014 was the highest on record (19 mm; 1949–2014). The area affected by ROS events is expected to increase by 40% by the 2080s over Northern Eurasia [*Ye et al.*, 2008]. However, strong regional variability in ROS complicates generalizations about future ROS trends under a changing climate [*Cohen et al.*, 2015]. The increase of fall greenhouse soil gas production and the increase of spring ROS events suggest more frequent and/or larger spring pulses in the future that can offset the growing season carbon sink in the Arctic.

Acknowledgments
The Next-Generation Ecosystem Experiments (NGEE Arctic) project and the Atmospheric Radiation Measurement Program are supported by the Office of Biological and Environmental Research in the DOE Office of Science. Snow depth and density were measured with the support of Arctic Landscape Conservation Cooperative, U.S. Fish and Wildlife Service project ALCC2012-07.

References

Belshe, E. F., E. A. G. Schuur, and B. M. Bolker (2013), Tundra ecosystems observed to be CO2 sources due to differential amplification of the carbon cycle, *Ecol. Lett.*, *16*(10), 1307–1315, doi:10.1111/ele.12164.

Billesbach, D. P. (2011), Estimating uncertainties in individual eddy covariance flux measurements: A comparison of methods and a proposed new method, *Agric. For. Meteorol.*, *151*(3), 394–405, doi:10.1016/j.agrformet.2010.12.001.

Brown, J., P. C. Miller, L. L. Tieszen, and F. Bunnell (1980), *An Arctic Ecosystem: The Coastal Tundra at Barrow, Alaska, Dowden*, Huchinson and Ross Inc., Penssylvania, doi:10.1575/1912/222.

Bubier, J., P. Crill, and A. Mosedale (2002), Net ecosystem CO2 exchange measured by autochambers during the snow-covered season at a temperate peatland, *Hydrol. Processes*, *16*(18), 3667–3682, doi:10.1002/hyp.1233.

Cohen, J., H. Ye, and J. Jones (2015), Trends and variability in rain-on-snow events, *Geophys. Res. Lett.*, *42*, 7115–7122, doi:10.1002/2015GL065320.

Fahnestock, J. (1999), Wintertime CO2 efflux from arctic soils: Implications for annual carbon budgets, *Global Biogeochem. Cycles*, *13*(3), 775–779, doi:10.1029/1999GB900006.

Friborg, T., T. R. Christensen, and H. Søgaard (1997), Rapid response of greenhouse gas emission to early spring thaw in a subarctic mire as shown by micrometeorological techniques, *Geophys. Res. Lett.*, *24*(23), 3061–3064, doi:10.1029/97GL03024.

Gangodagamage, C., et al. (2014), Extrapolating active layer thickness measurements across Arctic polygonal terrain using LiDAR and NDVI data sets, *Water Resour. Res.*, *50*, 6339–6357, doi:10.1002/2013WR014283.

Hargreaves, K. J., D. Fowler, C. E. R. Pitcairn, and M. Aurela (2001), Annual methane emission from Finnish mires estimated from eddy covariance campaign measurements, *Theor. Appl. Climatol.*, *70*(1–4), 203–213, doi:10.1007/s007040170015.

Hubbard, S. S., et al. (2012), Quantifying and relating land-surface and subsurface variability in permafrost environments using LiDAR and surface geophysical datasets, *Hydrogeol. J.*, *21*(1), 149–169, doi:10.1007/s10040-012-0939-y.

Hugelius, G., et al. (2014), Estimated stocks of circumpolar permafrost carbon with quantified uncertainty ranges and identified data gaps, *Biogeosciences*, *11*, 6573–6593, doi:10.5194/bg-11-6573-2014.

Jansson, J. K., and N. Taş (2014), The microbial ecology of permafrost, *Nat. Rev. Microbiol.*, *12*(6), 414–25, doi:10.1038/nrmicro3262.

Lee, X., W. Massman, and B. Law (2004), *Handbook of Micrometeorology: A Guide for Surface Flux Measurement and Analysis, Atmos. Oceanogr. Sci. Lib.*, vol. 29, Springer, Dordrecht, Netherlands.

Mastepanov, M., C. Sigsgaard, E. J. Dlugokencky, S. Houweling, L. Ström, M. P. Tamstorf, and T. R. Christensen (2008), Large tundra methane burst during onset of freezing, *Nature*, *456*(7222), 628–630, doi:10.1038/nature07464.

Mastepanov, M., C. Sigsgaard, T. Tagesson, L. Ström, M. P. Tamstorf, M. Lund, and T. R. Christensen (2013), Revisiting factors controlling methane emissions from high-Arctic tundra, *Biogeosciences*, *10*(7), 5139–5158, doi:10.5194/bg-10-5139-2013.

McGuire, A. D., et al. (2012), An assessment of the carbon balance of Arctic tundra: Comparisons among observations, process models, and atmospheric inversions, *Biogeosciences*, *9*(8), 3185–3204, doi:10.5194/bg-9-3185-2012.

Moore, T. R., and R. Knowles (1990), Methane emissions from fen, bog and swamp peatlands in Quebec, *Biogeochemistry*, *11*(1), 45–61, doi:10.1007/BF00000851.

Natali, S., et al. (2015), Permafrost thaw and soil moisture drive CO2 and CH4 release from upland tundra, *J. Geophys. Res. Biogeosci.*, *120*, 525–537, doi:10.1002/2014JG002872.

Nykänen, H., J. E. P. Heikkinen, L. Pirinen, K. Tiilikainen, and P. J. Martikainen (2003), Annual CO2 exchange and CH 4 fluxes on a subarctic palsa mire during climatically different years, *Global Biogeochem. Cycles*, *17*(1), 1018, doi:10.1029/2002GB001861.

Oechel, W. C., G. Vourlitis, and S. J. Hastings (1997), Cold season CO2 emission from Arctic soils, *Global Biogeochem. Cycles*, *11*(2), 163–172, doi:10.1029/96GB03035.

Oechel, W. C., C. A. Laskowski, G. Burba, B. Gioli, and A. A. M. Kalhori (2014), Annual patterns and budget of CO2 flux in an Arctic tussock tundra ecosystem, *J. Geophys. Res. Biogeosci.*, *119*, 323–339, doi:10.1002/2013JG002431.

Orsi, T. H., A. L. Anderson, and A. P. Lyons (1996), X-ray tomographic analysis of sediment macrostructure in Eckernforde Bay, western Baltic Sea, *Geo-Mar. Lett.*, *16*(3), 232–239, doi:10.1007/BF01204514.

Pirk, N., T. Santos, C. Gustafson, A. J. Johansson, F. Tufvesson, F. J. W. Parmentier, M. Mastepanov, and T. R. Christensen (2015), Methane emission bursts from permafrost environments during autumn freeze-in: New insights from ground-penetrating radar, *Geophys. Res. Lett.*, *42*, 6732–6738, doi:10.1002/2015GL065034.

Reichstein, M., et al. (2005), On the separation of net ecosystem exchange into assimilation and ecosystem respiration: Review and improved algorithm, *Global Change Biol.*, *11*(9), 1424–1439, doi:10.1111/j.1365-2486.2005.001002.x.

Romanovsky, V. E., and T. E. Osterkamp (2000), Effects of unfrozen water on heat and mass transport processes in the active layer and permafrost, *Permafrost Periglacial Process.*, *11*(3), 219–239, doi:10.1002/1099-1530(200007/09)11:3<219:AID-PPP352>3.0.CO;2-7.

Schadel, C., et al. (2016), Potential carbon emissions dominated by carbon dioxide from thawed permafrost soils, *Nat. Clim. Change*, *6*, 950–953, doi:10.1038/nclimate3054.

Schuur, E. A. G., et al. (2015), Climate change and the permafrost carbon feedback, *Nature*, *520*, 171–179, doi:10.1038/nature14338.

Song, C., X. Xu, X. Sun, H. Tian, L. Sun, Y. Miao, X. Wang, and Y. Guo (2012), Large methane emission upon spring thaw from natural wetlands in the northern permafrost region, *Environ. Res. Lett.*, *7*(3), 34009, doi:10.1088/1748-9326/7/3/034009.

Spielhagen, R. F., K. Werner, S. A. Sørensen, K. Zamelczyk, E. Kandiano, G. Budeus, K. Husum, T. M. Marchitto, and M. Hald (2011), Enhanced modern heat transfer to the Arctic by warm Atlantic Water, *Science*, *331*(6016), 450–453, doi:10.1126/science.1197397.

Sturtevant, C. S., and W. C. Oechel (2013), Spatial variation in landscape-level CO2 and CH4 fluxes from arctic coastal tundra: Influence from vegetation, wetness, and the thaw lake cycle, *Global Change Biol.*, *19*(9), 2853–66, doi:10.1111/gcb.12247.

Tagesson, T., M. Mölder, M. Mastepanov, C. Sigsgaard, M. P. Tamstorf, M. Lund, J. M. Falk, A. Lindroth, T. R. Christensen, and L. Ström (2012), Land-atmosphere exchange of methane from soil thawing to soil freezing in a high-Arctic wet tundra ecosystem, *Global Change Biol.*, *18*(6), 1928–1940, doi:10.1111/j.1365-2486.2012.02647.x.

Taina, I. A., R. J. Heck, and T. R. Elliot (2008), Application of X-ray computed tomography to soil science: A literature review, *Can. J. Soil Sci.*, *88*(1), 1–19, doi:10.4141/CJSS06027.

Tokida, T., M. Mizoguchi, T. Miyazaki, A. Kagemoto, O. Nagata, and R. Hatano (2007), Episodic release of methane bubbles from peatland during spring thaw, *Chemosphere*, *70*(2), 165–171, doi:10.1016/j.chemosphere.2007.06.042.

Torn, M., and F. Chapin (1993), Environmental and biotic controls over methane flux from arctic tundra, *Chemosphere*, *26*(1–4), 357–368.

Ueyama, M., H. Iwata, Y. Harazono, E. S. Euskirchen, W. C. Oechel, and D. Zona (2013), Growing season and spatial variations of carbon fluxes of Arctic and boreal ecosystems in Alaska (USA), *Ecol. Appl.*, *23*(8), 1798–1816, doi:10.1890/11-0875.1.

von Fischer, J. C., R. C. Rhew, G. M. Ames, B. K. Fosdick, and P. E. von Fischer (2010), Vegetation height and other controls of spatial variability in methane emissions from the Arctic coastal tundra at Barrow, Alaska, *J. Geophys. Res.*, *115*, G00I03, doi:10.1029/2009JG001283.

Walter, K. M., L. C. Smith, and F. S. Chapin (2007), Methane bubbling from northern lakes: Present and future contributions to the global methane budget, *Philos. Trans. R. Soc., A*, *365*(1856), 1657–76, doi:10.1098/rsta.2007.2036.

Wille, C., L. Kutzbach, T. Sachs, D. Wagner, and E.-M. Pfeiffer (2008), Methane emission from Siberian arctic polygonal tundra: Eddy covariance measurements and modeling, *Global Change Biol.*, *14*(6), 1395–1408, doi:10.1111/j.1365-2486.2008.01586.x.

Windsor, J., T. R. Moore, and N. T. Roulet (1992), Episodic fluxes of methane from subarctic fens, *Can. J. Soil Sci.*, *72*(4), 441–452, doi:10.4141/cjss92-037.

Wullschleger, S. D., H. E. Epstein, E. O. Box, E. S. Euskirchen, S. Goswami, C. M. Iversen, J. Kattge, R. J. Norby, P. M. van Bodegom, and X. Xu (2014), Plant functional types in Earth system models: Past experiences and future directions for application of dynamic vegetation models in high-latitude ecosystems, *Ann. Bot.*, *114*(1), 1–16, doi:10.1093/aob/mcu077.

Yang, D., B. E. Goodison, and S. Ishida (1998), Adjustment of daily precipitation data at 10 climate stations in Alaska: Applications of World Meteorological Organization intercomparison results, *Water Resour. Res.*, *34*(2), 241–256, doi:10.1029/97WR02681.

Ye, H., D. Yang, and D. Robinson (2008), Winter rain on snow and its association with air temperature in northern Eurasia, *Hydrol. Processes*, *22*(15), 2728–2736.

Zona, D., et al. (2015), Cold season emissions dominate the Arctic tundra methane budget, *Proc. Natl. Acad. Sci. U.S.A.*, *113*(1), 40–45, doi:10.1073/pnas.1516017113.